Transport properties of energetic particles in a turbulent electrostatic field

G. Manfredi and R. O. Dendy
UKAEA Fusion, Culham (UKAEA/Euratom Fusion Association), Abingdon, Oxfordshire, OX14 3DB, United Kingdom

(Received 28 August 1996; accepted 21 November 1996)

The diffusion of test particles in a turbulent electrostatic field is investigated numerically. The field is obtained by solving the Hasegawa–Mima model for two-dimensional drift turbulence. It is shown that nonlinear coupling significantly reduces the level of transport compared to the linear regime, and the physical mechanisms leading to this effect are analyzed in detail. Finite Larmor radius effects, relevant to alpha-particle transport in tokamaks, also reduce the diffusion rate. The scaling of the diffusion coefficient with Larmor radius is derived from a closure theory, and the predictions are compared to results from computer experiments. It is suggested that measured diffusion rates of particles with different Larmor radii can be used to obtain information about the turbulence. [S1070-664X(97)00703-9]

I. INTRODUCTION

Electrostatic drift turbulence is believed to play an important role in the physics of magnetized plasmas.[1–4] It is dominated by the $\mathbf{E}\times\mathbf{B}$ drift, and involves low-frequency waves, which are driven unstable by the presence of a temperature or density gradient. At present, drift turbulence is a promising candidate to explain from first principles the high levels of energy and particle transport observed in tokamaks (anomalous transport). Recent results from realistic kinetic and fluid simulations seem to support this conjecture.[5–9]

On the other hand, a good understanding of the confinement properties of energetic alpha particles is of growing importance as tokamak plasmas approach the ignition regime.[10] Because the Larmor radii of alpha particles born in fusion reactions greatly exceed those of the thermal ions, their response to a turbulent field in the plasma can be significantly different. For example, the larger scale of gyro and drift motion will smooth out the effects of short wavelength turbulence, creating a differential response for particles of different energies. Given a theoretical understanding of this differential effect, observations of alpha-particle transport may yield information on the characteristics of the turbulence.[11]

Here, we shall consider the general plasma physics question of the impact of nonlinear coupling and finite Larmor radius on test particle transport in strong electrostatic drift turbulence. As a simple paradigm for drift turbulence we shall use the Hasegawa–Mima equation,[4] whose scope and limitations are discussed in Sec. II. It incorporates both strong nonlinearity and linear dispersion in its description of the drift turbulent electrostatic field, thus going beyond the existing literature dealing with the stochastic diffusion induced by a collection of linearly independent drift waves.[12–16] In addition, most earlier work does not take into account finite Larmor radius effects, whose impact on the particle transport will be one of our main concerns in this paper.

Early numerical studies reported results either for a small number of waves,[12] or for many waves oscillating at the same frequency[13] (while, for real drift waves, frequency and wave number are not independent, but obey a simple dispersion relation). In more recent studies,[16] the correlation length (λ_c) and time (τ_c) of a stochastic $\mathbf{E}\times\mathbf{B}$ field are specified, and the author determines the scaling of the diffusion coefficient with the Kubo number $K=v_E\tau_c/\lambda_c$, where v_E measures the amplitude of the velocity field. Early theoretical results were based on a closure approximation,[17] in which the electric field is assumed to have Gaussian statistical properties in wave number space. With this assumption, the diffusion coefficient can be computed from the field spectrum, which gives correct results in the quasilinear regime ($D\propto K$ for $K\ll 1$). In the opposite limit of large Kubo numbers, closure theory predicts the diffusion coefficient to be independent of K. This is obviously incorrect, since $K=\infty$ corresponds to a ''frozen'' field, which, in two dimensions, only allows for closed, periodic orbits, and therefore no diffusion. More sophisticated results,[18,19] derived from percolation theory, reproduce the correct behavior within good accuracy, as was verified in the simulations reported in Ref. 16.

The above studies give a satisfactory picture of the stochastic diffusion of test particles with zero Larmor radius in a field composed of *linearly independent* waves. However, these studies disregard the fact that such waves interact nonlinearly with one another, and this greatly restricts their range of applicability, especially when considering large amplitude waves. Nonlinear effects can, in principle, profoundly alter the spectrum of the electrostatic field and therefore lead to substantially different diffusion rates. Recently,[11] we showed that, for a simple model of two-dimensional strong drift turbulence, nonlinear couplings virtually suppress the diffusion of test particles. In the present paper, we provide more evidence about this phenomenon, and try to identify a mechanism leading to it. Our interpretation is that strongly nonlinear couplings rapidly modify the initial spectrum during the very early stages of the evolution. The modified spectrum arising from this early phase is one that leads to mainly periodic orbits, and very weak diffusion.

The present paper is organized as follows. In the next section, we describe the model we adopt for strong drift turbulence, namely the Hasegawa–Mima equation. Section III contains the main numerical results and their interpretation. In Sec. IV we discuss the impact of large Larmor radius on

particle transport, and show how knowledge of this effect can be utilized to infer properties of the turbulent field. Conclusions are drawn in Sec. V.

II. A BASIC MODEL FOR DRIFT TURBULENCE

Our aim is to analyze the motion of test particles in a strongly turbulent magnetized plasma. In order to do so, we need a nonlinear model for drift turbulence in real space, whose output is the time-dependent electrostatic potential. The potential will then act as an input for the equation of motion of the test particle guiding centers, which follow the $\mathbf{E}\times\mathbf{B}$ drift: $d\mathbf{r}/dt=\mathbf{B}\times\nabla\phi/B^2$. This motion is thus uniquely determined by the turbulent field at all times. It is worth noticing that the equations of motion are Hamiltonian in form, with the real space (x,y) coinciding with the phase space, and $H(x,y,t)=\phi(x,y,t)/B$. Our technique for extending this approach to the case of finite Larmor radius is described in Sec. IV.

For the sake of simplicity, and to concentrate on the relevant issues, we adopt here a long-established model for drift turbulence, the Hasegawa–Mima (HM) equation:[4]

$$\frac{\partial}{\partial t}(\phi-\nabla^2\phi)-[\nabla\phi\times\mathbf{e}_z\cdot\nabla]\nabla^2\phi=\frac{\partial\phi}{\partial x}. \tag{1}$$

This equation describes two-dimensional drift turbulence in the plane perpendicular to the magnetic field direction $\mathbf{e}_z$, and can be derived from the ion continuity equation with $\mathbf{E}\times\mathbf{B}$ and polarization drifts, and assuming an adiabatic response for the electrons. Time is normalized to L_n/C_s ($C_s=\sqrt{T_e/m_i}$ is the sound speed), space to the thermal Larmor radius $\rho_s=C_s\Omega_i^{-1}$ ($\Omega_i=eB/m_i$), and the potential to $(T_e/e)(\rho_s/L_n)$; L_n is a typical scale of variation of the equilibrium density profile. The generalized vorticity $W=\phi-\nabla^2\phi$ is the actual quantity transported by the flow. The linear limit of Eq. (1) is equivalent to the evolution of a collection of independent drift waves obeying the (dimensionless) dispersion relation $\omega_{\mathbf{k}}=k_x/(1+k^2)$. The computational box is periodic in the x direction ($0<x<L_x$) and finite in y ($-L_y<y<L_y$; both ϕ and W vanish at $y=\pm L_y$). A dissipative term, of the form $\nu\nabla^2 W$, is added to the right-hand side of Eq. (1) to control the numerical noise at small wavelengths, although no forcing is included at this stage (freely decaying turbulence). The initial condition is taken to be a random vorticity distribution

$$W(x,y,t=0)=\sum_n\sum_m\frac{A}{(n^2+m^2)^{1/2}}\times\sin\left[\frac{\pi}{2L_y}m(y-L_y)\right]\cos\left(\frac{2\pi}{L_x}nx+\beta_{mn}\right), \tag{2}$$

where β_{mn} are random phases and A is the amplitude. This choice corresponds to a spectrum $|\phi_k|\propto k^{-3}$.

Although the HM model Eq. (1) captures some of the basic properties of drift waves, such as the dispersion relation and the main nonlinearities, it is important to be aware of its limitations. In particular, the HM equation assumes cold ions (thus ruling out finite gyroradius effects), perfect adiabatic response for the electrons, and purely two-dimensional (2D) turbulence. The first two hypotheses should not affect our main conclusions on the transport of test particles. Three-dimensionality might play an important role. For example, the existence of an inverse cascade (energy condensing at the smallest wave number) is a typical feature of 2D turbulence,[20,21] and this may affect the diffusion of test particles. A second, important difference is that, in three-dimensions (3D), a time-independent field can trigger test particle diffusion, whereas this is forbidden in 2D. At present, the stochastic diffusion of test particles in a 3D field is a largely unexplored domain, which certainly deserves future investigation. Despite these limitations, one must bear in mind that, since magnetized plasmas are strongly anisotropic, the 2D assumption is often a reasonably good approximation. In the present paper, we have not included a source (forcing) term for the turbulence. Such a term was included in our treatment in Ref. 11, to which we refer for details: for that particular choice of source terms, the results were basically the same as for the freely decaying turbulence considered here. The number of instabilities that could generate the turbulence is very large, and the mathematical formulation and parametrization of the corresponding source terms would be very varied. Omission of a source term thus has the further benefit, for the present general plasma physics purposes, of minimizing the number of free parameters and enabling us to isolate the basic problem of particle transport in the turbulent field. It can also be seen from the simulations below that the particle diffusion time exceeds the turbulence decay time $1/\nu$ by at least an order of magnitude, so that the turbulent state is effectively stationary for each test particle.

III. NUMERICAL RESULTS

In a recent communication,[11] we showed that nonlinear field coupling greatly reduces particle transport. Let us now try to identify the main mechanisms leading to the suppression of diffusion. In the present example the sums in Eq. (2) are in the ranges $2\leqslant m\leqslant 10$, $2\leqslant n\leqslant 10$, with $L_x=2L_y=20\rho_s$ and $\nu=0.001D_{\mathrm{GB}}$, where $D_{\mathrm{GB}}=\rho_s^3\Omega_i/L_n$ is the gyro-Bohm diffusion coefficient. The test particles are initially located in a narrow band around $y=0$, and uniformly distributed in x. After following the trajectories of 3000 particles, we compute several statistical quantities. In particular, the mean square displacement $Y^2(t)$, the diffusion coefficient in the y (nonperiodic) direction $D_y(t)$, and the kurtosis $K(t)$ are defined by

$$D_y(t)=\frac{Y^2(t)}{2t}=\frac{\langle[y(t)-y(0)]^2\rangle}{2t},$$
$$K(t)=\frac{\langle[y(t)-y(0)]^4\rangle}{3\langle[y(t)-y(0)]^2\rangle^2}, \tag{3}$$

where the angular brackets denote an average over all particles, and $K=1$ for a Gaussian distribution. For a truly diffusive process, the diffusion coefficient should be asymptotically time independent.

The time history of $Y^2(t)$ is plotted in Fig. 1, both for the linear and the nonlinear cases, showing clearly that nonlinear coupling does suppress the diffusion. The kurtosis,

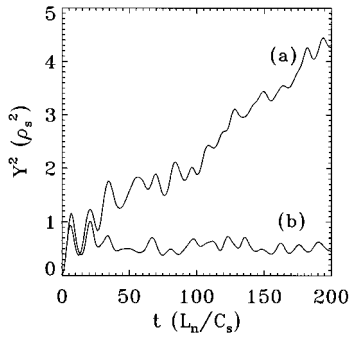

FIG. 1. Mean square particle displacement in the nonperiodic direction for the linear (a) and nonlinear (b) case.

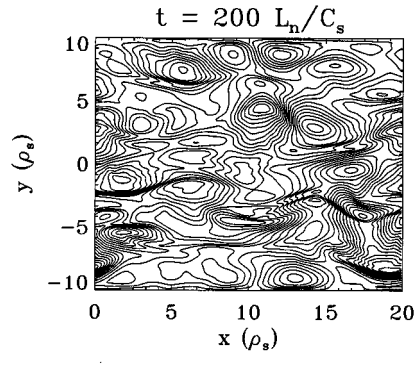

FIG. 3. Contour plot of the generalized vorticity at the end of the nonlinear evolution. Elongated structures parallel to the x axis are visible.

after a short transient, takes a value close to unity for both cases (Fig. 2). In Ref. 11, we attributed the suppression of stochastic diffusion to the large scale structures that are created in the nonlinear evolution as a result of the inverse cascade. As mentioned in Sec. I, this is essentially a two-dimensional effect, closely related to the conservation of enstrophy. These large scale structures are clearly visible from the vorticity contours at $t=200L_n/C_s$ (Fig. 3, compare with Fig. 4 which results from the linear evolution). Their impact on the level of transport may be due to the fact that, for long wavelengths, all linear waves propagate with the same phase velocity, which can be eliminated by a Galilean transformation, thus suppressing all time dependence in the potential. The nonlinear terms are also negligible when $\rho_s k_x \ll 1$. Therefore, particles trapped in these large vortices follow the field lines adiabatically, and are less likely to ''jump'' from one vortex to another; nonadiabatic motion is indeed recognized as the origin of stochastic diffusion.[12]

More precisely, we conjecture that the nonlinear terms in the HM equation induce a rapid transition in the field spectrum at an early stage of the evolution. At the end of this transition, the nonlinear terms have become negligible (because long wavelengths dominate): however, the field emerging from this process is, for the same reason, one that leads to very low particle transport.

In order to verify this conjecture, we perform the following numerical experiment. The nonlinear simulation is stopped at $t=200L_n/C_s$; the particle positions are reinitialized around $y=0$; then the simulation is restarted from the state to which it has evolved, but now suppressing the nonlinear terms. In practice, we are doing a linear simulation in which the initial condition is the one of Fig. 3. If our conjecture is correct, the subsequent evolution should lead to a very small diffusion coefficient even if the nonlinear terms are not present: this would mean that the above-mentioned transition is already completed at $t=200L_n/C_s$. The results, shown in Fig. 5, confirm our prediction [Fig. 5(b)]. In order to avoid all spurious effects (due, for example, to dissipation), the same experiment has been conducted on the originally linear simulation, the one leading to the vorticity field of Fig. 4. As expected, in this case diffusion takes place [Fig. 5(a)], although at a smaller rate than in Fig. 1, because the field has been decaying from $t=0$ to $t=200L_n/C_s$ due to the viscous term (in this case, $\nu=0.001D_{\mathrm{GB}}$). Finally, if we keep the nonlinear terms throughout the second phase of the experiment, we again observe no diffusion [Fig. 5(c)], just as in the case of Fig. 5(b). This reinforces our belief that, after the transition has occurred, the nonlinear terms play a negligible role. These results are even more compelling if we greatly reduce the viscosity in the second phase of the simulation ($\nu=0.0001D_{\mathrm{GB}}$), which is feasible since the nonlinear terms are suppressed (Fig. 6).

The same experiment is repeated by stopping the simulation at $t=50L_n/C_s$ and reinitializing the particles as above (Fig. 7). In this case, the transition is not complete, and some

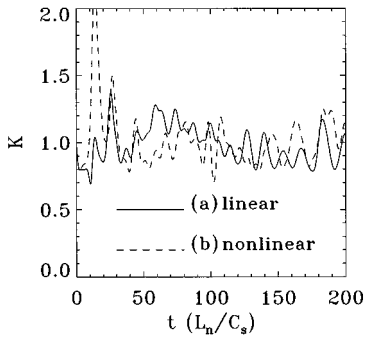

FIG. 2. Time evolution of the kurtosis in the same case as Fig. 1. The solid curve (a) refers to the linear case and the broken curve (b) to the nonlinear one. For a Gaussian distribution of particles the kurtosis is equal to one.

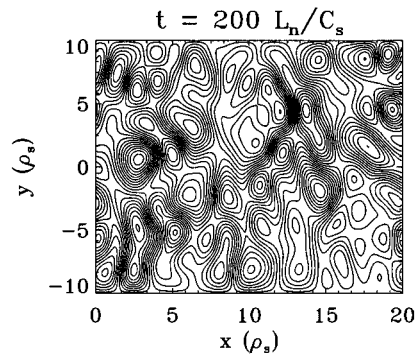

FIG. 4. Contour plot of the generalized vorticity at the end of the linear evolution. No anisotropy is observed.

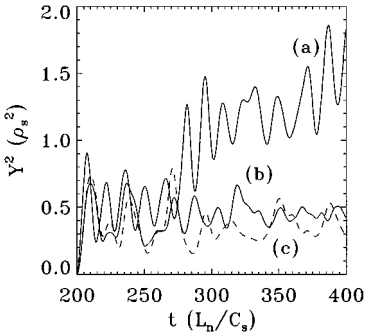

FIG. 5. Mean square particle displacement in the nonperiodic direction. The linear and nonlinear runs of Fig. 1 have been stopped at $t=200L_n/C_s$ and then restarted from their evolved state, but suppressing the nonlinear terms. Case (a) comes from the originally linear run and case (b) from the originally nonlinear run. Case (c) (broken line) is the continuation of the nonlinear run, including the nonlinear terms.

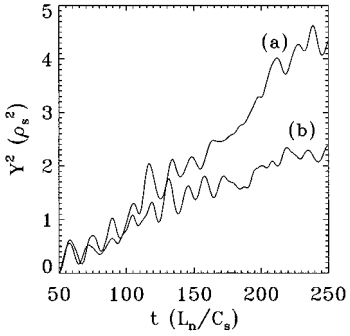

FIG. 7. The same computer experiment as Figs. 5(a) and 5(b), but restarting the run at $t=50L_n/C_s$. Case (a) comes from the originally linear run and case (b) from the originally nonlinear run. Some residual diffusion is now observed in case (b).

residual diffusion is still observed in the simulation which uses the field arising from the nonlinear evolution [Fig. 7(b)].

When nonlinearities are present, the test particle motion shows highly coherent patterns. This is clearly illustrated by initially locating the particles within a small square at the center of the computational domain, with a uniform distribution. Since the particle motion is Hamiltonian, the area of the square is preserved, although its shape is free to change. Chaotic motion, and stochastic diffusion, arise when the shape of the square is so distorted and intricate that, when allowance is made for coarse graining arising from the discreteness of the particles, its effective surface area is much larger than the original area of the square. This is what happens in the case of linear evolution (Fig. 8): after some time, the original shape is lost and stochastic diffusion takes place. For nonlinear evolution (Fig. 9), in contrast, the coherence of the motion is preserved over the entire simulation. The shape is deformed, but never loses its identity as a single object. This clearly indicates that nonlinear effects preclude the possibility of chaotic trajectories for the particles.

The importance of nonlinear effects in Eq. (1) is determined by the amplitude A in Eq. (2) and by the spectrum of the initial vorticity distribution. For the same spectrum, a smaller value of A corresponds to weaker nonlinear effects, and the solution of Eq. (1) should be closer to that obtained in the corresponding linear case. On the other hand, the diffusion coefficient also scales with the amplitude (for example, in the quasilinear regime, $D\propto A^2$). In order to compare the relative strength of these two competing effects, we performed a simulation with $A=0.5$ (in the previous examples we had $A=1$). It turns out that nonlinear effects are

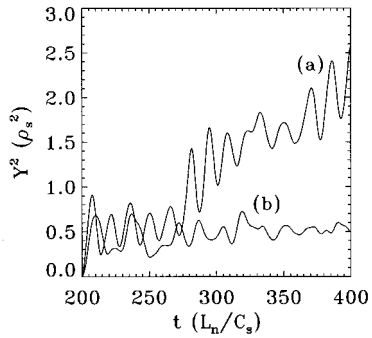

FIG. 6. The same computer experiment as Figs. 5(a) and (b), but with a smaller viscosity $\nu=10^{-4}D_{GB}$. Both cases are linear from $t=200L_n/C_s$ on, but case (a) was also linear from $t=0$ to $t=200L_n/C_s$, while (b) was nonlinear.

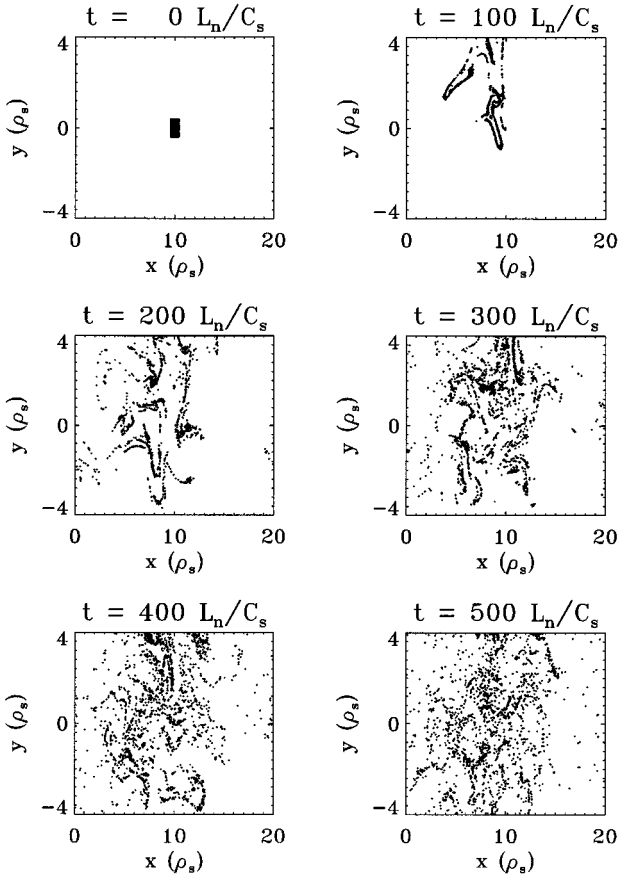

FIG. 8. Particle distribution for a typical linear case. Although the area of the original small box is preserved, chaotic motion spreads the particles over the entire computational domain.

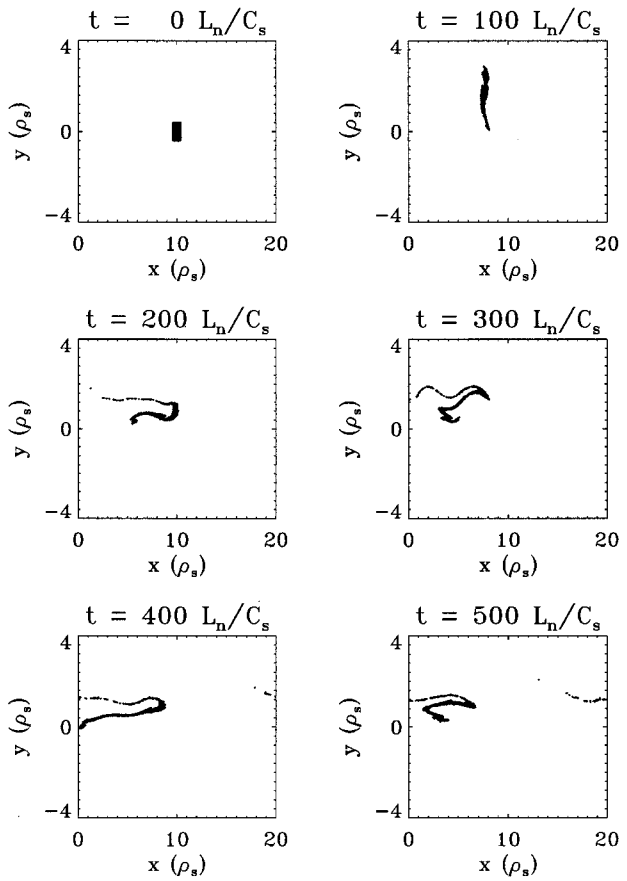

FIG. 9. Particle distribution for a typical nonlinear case. Particle trajectories are not chaotic, and coherent motion is observed.

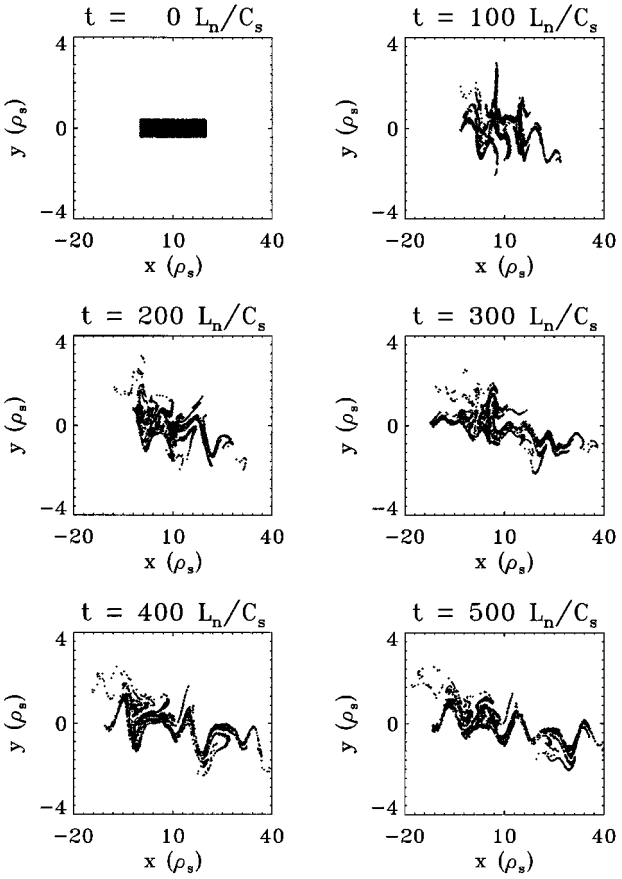

FIG. 11. Particle distribution in a nonlinear case. The computational domain extends from $x=0$ to $x=L_x=20\rho_s$, but the particles are allowed to leave the periodic domain in order to visualize their motion in x. Particles travel longer distances in x than in y.

still strong enough to prevent particle diffusion. The same result is obtained with a larger amplitude $A=2$, which corroborates the hypothesis that nonlinear effects, however small, lead eventually to coherent, nondiffusive motion.

So far, we have concentrated our attention on the diffusion in the nonperiodic direction y. Turning to the periodic direction x, which is the direction perpendicular to the equilibrium density gradient, we define the mean square displacement $X(t)$ through

$$X^2(t)=\langle[x(t)-\langle x(t)\rangle]^2\rangle. \tag{4}$$

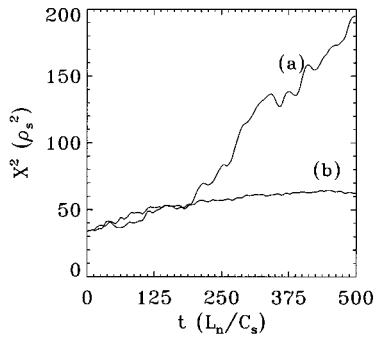

FIG. 10. Mean square particle displacement in the periodic direction x for the nonlinear (a) and linear (b) cases. Note that, contrarily to Y, X is larger in the nonlinear regime.

The time history of $X(t)$ is shown in Fig. 10, and reveals that the test particles travel a *longer* distance when nonlinear effects are switched on. This is the opposite of what was obtained in the y direction. There is, however, no contradiction, since the motion along x is not diffusive, but rather coherent, as shown in Fig. 11, where the patterns of the underlying field are clearly revealed by the particle trajectories. Thus, the coherent motion occurring in the nonlinear regime allows the particles to travel for short distances in y, but much longer distances in x. This anisotropic effect arises from an asymmetry in the original HM equation, in which the two coordinates are not equivalent, since the equilibrium density gradient is directed along the y axis. Contour plots of the vorticity also reveal the presence of structures elongated in the x direction (Fig. 3). The anisotropy of the turbulence can be quantified by comparing the average unidirectional vorticity spectra

$$\overline{W_{k_x}}=\int_{-L_y}^{L_y}|W_{k_x}(y)|dy, \quad \overline{W_{k_y}}=\int_{0}^{L_x}|W_{k_y}(x)|dx, \tag{5}$$

where, for example $W_{k_x}(y)$ is obtained from $W(x,y)$ by Fourier transforming over x. The spectra defined in Eq. (5) are plotted in Figs. 12 and 13, and show that short scales are

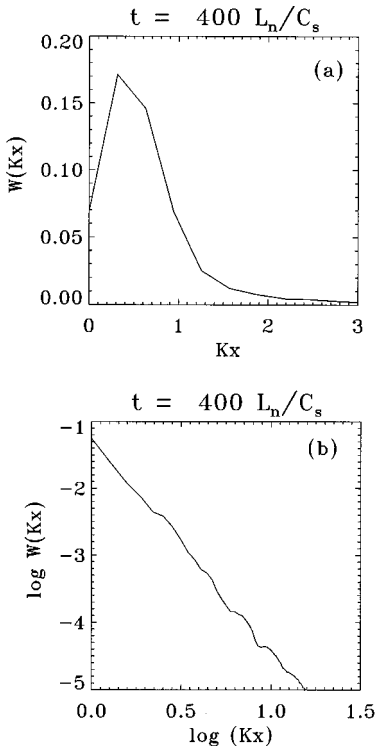

FIG. 12. Unidirectional x spectrum of the vorticity as defined in Eq. (5) on a linear scale (a) and a logarithmic scale (base 10) (b). Large scale structures are more strongly excited.

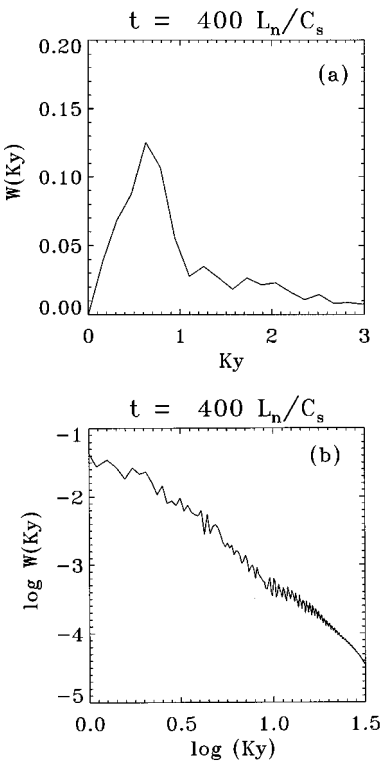

FIG. 13. Unidirectional y spectrum of the vorticity as defined in Eq. (5) on a linear scale (a) and a logarithmic scale (base ten) (b). The peak observed in (a) is centered at a higher wave number compared to the x spectrum of Fig. 12(a). Small scale structures are globally more strongly excited.

more strongly excited in the direction of the density gradient, y. The mean square wave numbers in each direction are $\langle k_x^2\rangle^{1/2}=1.27$ and $\langle k_y^2\rangle^{1/2}=3.87$.

The different spectra reflect the existence of different correlation lengths for the two directions. It should also be noted that, due to the different boundary conditions, open flow lines can only exist in the x direction, and we have indeed observed some of them in the vorticity contours. Along an open flow line, the correlation length is virtually infinite, and, for a frozen field, a particle moving on such a line would travel an infinite distance in x, with a finite excursion in y.

This behavior is a signature of the so-called ''zonal flows,'' or elongated structures in the direction perpendicular to the density gradient, which are visible in Fig. 3. In an early paper, Hasegawa, Maclennan, and Kodama[22] speculated that zonal flows may inhibit particle transport across the flow, and our numerical results support such a conjecture.

IV. FINITE LARMOR RADIUS (FLR) EFFECTS

For energetic alpha-particles, the guiding-center model described above is no longer valid, and effects due to their large Larmor radii must be taken into account. The simplest model for FLR is obtained by ''spreading'' the particle over a ring centered at the position of its guiding-center, and it is accurate as long as the gyration frequency $\Omega_i=eB/m_i$ is much larger than the drift frequency $\omega_\star=\Omega_i\rho_s/L_n$. This model can be implemented numerically by defining the electric field acting on a particle as the average field calculated at $N_{\rm gyro}$ points distributed over a ring whose radius is equal to the Larmor radius.[23] The averaging operation tends to suppress the smaller-scale components of the electric field (a similar effect could arise from the banana orbits, induced by the inhomogeneity of the magnetic field in tokamak geometry). This point has been raised in the context of electron diffusion in a stochastic magnetic field.[24] We have already shown[11] how FLR can greatly reduce the transport of test particles. We now try to quantify this reduction more precisely, and suggest a computer experiment in which this effect is used to extract information about the underlying turbulent field.

According to the closure theory of Refs. 13 and 17, the test particle diffusion coefficient takes one of the following dimensionless forms, in the quasilinear (small amplitude) and frozen turbulence (large amplitude) regimes, respectively:

$$D^2\propto\sum_k \frac{1}{\omega_k^2}\langle \mathbf{E}_\mathbf{k}(t)\cdot\mathbf{E}_{-\mathbf{k}}(0)\rangle^2, \tag{6a}$$

$$D^2\propto\sum_k \frac{1}{k^2}\langle \mathbf{E}_\mathbf{k}(t)\cdot\mathbf{E}_{-\mathbf{k}}(0)\rangle, \tag{6b}$$

where now angular brackets denote average over the random phases. Thus the diffusion coefficient scales as the square of the field amplitude in the quasilinear regime, and linearly in the amplitude in the frozen turbulence regime. The name ''frozen turbulence'' is a reminder that the limit of large amplitudes is equivalent to that of small wave frequencies.

The more sophisticated results of Refs. 16, 18, and 19 predict a dependence slightly weaker than linear in the large amplitude case ($D \propto |E|^{0.7}$). However, the important point is that two different regimes can be clearly distinguished.

It can be shown[25] that our model for finite Larmor radius is equivalent to replacing the true field spectrum $\mathbf{E_k}$ with an effective $J_0(\rho k)\mathbf{E_k}$, where J_0 is a Bessel function and ρ is the Larmor radius. This enables us to scale the diffusion coefficient with Larmor radius, at least in the limit $\rho k \gg 1$, for which the Bessel function can be expanded as $J_0(\rho k) \propto (\rho k)^{-1/2}$. Thus, in the limit of large Larmor radii, the diffusion coefficient scales as ρ^{-1} in the quasilinear regime [Eq. (6a)], and as $\rho^{-1/2}$ in the frozen turbulence regime [Eq. (6b)]. Observation of the diffusion properties of alpha particles of different energies (and therefore different Larmor radii) should provide information about the turbulence and discriminate between the two regimes.

The effective amplitude of the velocity field is measured by a normalized amplitude a, which we now define. The root-mean square (rms) electric field is

$$E_{\mathrm{rms}}^2 = \langle |E|^2 \rangle = \frac{1}{2L_yL_x} \int_0^{L_x} dx \int_{-L_y}^{L_y} dy \; E^2(x,y,0); \qquad (7)$$

E_{rms} quantifies the amount of electric energy contained in the system. In a similar fashion, we also define a rms frequency $\omega_{\mathrm{rms}}^2 = \langle \omega_{\mathbf{k}}^2 \rangle$. Then, the normalized amplitude is given by the following expression:

$$a = \frac{2\pi}{L_x \omega_{\mathrm{rms}}} \frac{E_{\mathrm{rms}}}{B}. \qquad (8)$$

This definition is very close to the one used by Misguich *et al.*[17] in the case of a single frequency. In our first example, we set $A=25$, $L_x = 2L_y = 120$, which gives $a=0.36$, and therefore expect to be in the quasilinear regime. We have followed eight groups of particles with different Larmor radii. The measured diffusion coefficients are shown in Fig. 14(a) on a logarithmic scale. The slope$=-1$ line, corresponding to the quasilinear estimate, is a reasonably accurate fit to the computational curve, and certainly better then the slope$=-0.5$ line, which holds in the frozen turbulence regime. The oscillations arise from the behavior of the Bessel function J_0. When $A=100$, $L_x=120$, and $L_y=150$, the normalized amplitude is $a=1.24$, and Fig. 14(b) shows that the diffusion coefficient still scales as ρ^{-1}. For $a=2.45$ [Fig. 14(c)] we are at the boundary between the two regimes, while for $a=4.6$ [Fig. 14(d)] the diffusion coefficient scales as $\rho^{-1/2}$ as expected in the high-amplitude frozen turbulence case. In actuality, the slope$=-0.35$ line, which is the result obtained in Ref. 19 in the large amplitude limit, appears to give an even better fit, although it is difficult to discriminate between the two regimes.

In summary, we have been able to reconstruct some of the properties of a turbulent field simply by measuring the diffusion rates of test particles with different Larmor radii. It may be possible to devise techniques, based on this principle, which could be used to determine experimentally the level of turbulence in a magnetized plasma.

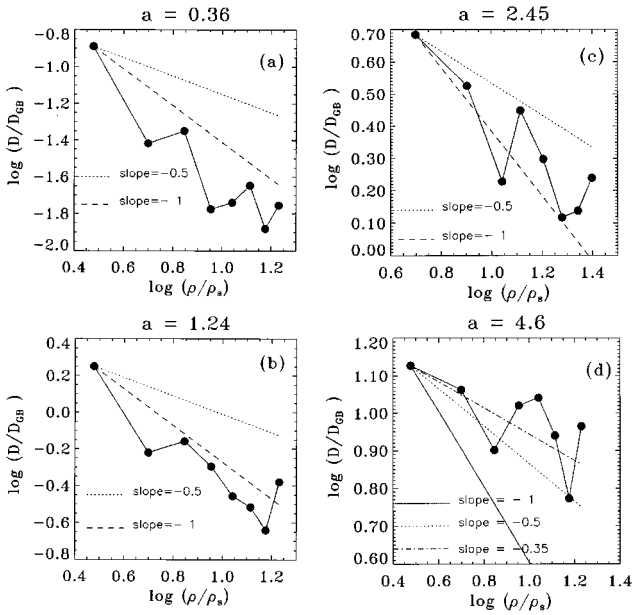

FIG. 14. Scaling of the diffusion coefficient against Larmor radius on a logarithmic scale (base 10) for four values of the normalized amplitude: $a=0.36$ (a); $a=1.24$ (b); $a=2.45$ (c); and $a=4.6$ (d). The slope$=-0.5$ line (dotted line) corresponds to the large amplitude scaling, while the slope$=-1$ line (broken line) corresponds to small amplitude scaling. In (d) the slope$=-0.35$ is also indicated, which corresponds to the result of Ref. 19 for large amplitude. The different regimes of small and large amplitude are clearly visible.

V. CONCLUSIONS

Anomalous transport in tokamak plasmas most probably arises from low-frequency, electrostatic, drift turbulence driven by ion-temperature-gradient instabilities. To date, it is not yet clear which kind of field spectra can be sustained by drift turbulence in a realistic three-dimensional, toroidal geometry. An open and important question, for example, is whether the dynamics will be essentially two-dimensional (due to the strong anisotropy induced by the magnetic field), or fully three-dimensional. An essentially 2D behavior can have a significant impact on the structure of the spectrum (2D turbulence admits an inverse energy cascade), and this in turn can profoundly influence the transport of test particles.

In this paper, we have discussed the impact of nonlinear coupling and finite Larmor radius on the transport of test particles. Our numerical results show that nonlinear field coupling can greatly reduce the particle diffusion coefficient. A detailed study of the physical mechanism leading to this effect shows that the nonlinear terms rapidly modify the field spectrum, and give rise to a new field which induces very small particle diffusion. This is therefore a practical example of how 2D turbulence can affect the transport of test particles.

By comparing the evolution of an initially localized packet of particles in a linear and nonlinear field, we have also shown that chaotic motion occurs only in the former case, while in the latter we observe regular, coherent patterns. The transport is found to possess different properties in the two directions perpendicular to the magnetic field. This anisotropy arises from a fundamental asymmetry in the

Hasegawa–Mima equation, reflecting the fact that along one of these directions (y) an equilibrium density gradient is present. The degree of anisotropy is quantified by means of the unidirectional field spectra, and the y spectrum is found to be peaked at a larger wave number, with small scale structures more strongly excited than in the x spectrum. This corresponds to the appearance of ''zonal flows'' parallel to the periodic direction x, which play a role in the nonlinear suppression of stochastic diffusion that we have observed.

Finally, we have investigated the impact of finite Larmor radius on test particle transport. The FLR effects must be taken into account when considering the transport of alpha particles which are born at high energy in fusion reactions. With the help of a simple picture for FLR and a theoretical model relating the diffusion coefficient to the structure of the electric field, it is possible to derive a scaling law for the diffusion coefficient against the Larmor radius. This scaling law varies according to the amplitude of the field, and thus enables us to discriminate between two different regimes: the quasilinear (or low amplitude) and the frozen turbulence (or high amplitude) regime. Computer experiments confirm the existence of these two regimes, and reproduce the scaling exponents predicted by the theory. Although our model does not include banana orbits, the results obtained appear to be generic and, in real experiments, this technique could be exploited to obtain information about the level of turbulence.

ACKNOWLEDGMENTS

The authors acknowledge helpful discussions with Dr. J. W. Connor and Dr. M. Ottaviani.

This work was partially funded by the Commission of the European Communities (Contract No. ERBCH-BICT941009), the UK Department of Trade and Industry and Euratom.

[1] P. C. Liewer, Nucl. Fusion **25**, 543 (1985).
[2] W. Horton, Phys. Rep. **192**, 1 (1990).
[3] J. W. Connor and H. R. Wilson, Plasma Phys. **36**, 719 (1994).
[4] A. Hasegawa and K. Mima, Phys. Fluids. **21**, 87 (1978).
[5] G. W. Hammett and F. W. Perkins, Phys. Rev. Lett. **64**, 3019 (1990).
[6] R. D. Sydora, T. S. Hahm, W. W. Lee, and J. M. Dawson, Phys. Rev. Lett. **64**, 2015 (1990).
[7] A. W. Dimits and W. W. Lee, Phys. Fluids B **3**, 1557 (1991).
[8] S. E. Parker, W. Dorland, R. A. Santoro, M. Beer, Q. P. Liu, W. W. Lee, and G. W. Hammett, Phys. Plasmas **1**, 1461 (1994).
[9] G. Manfredi, M. Shoucri, R. O. Dendy, A. Ghizzo, and P. Bertrand, Phys. Plasmas **3**, 202 (1996).
[10] R. K. Fisher, J. M. McChesney, P. B. Parks, H. H. Duong, S. S. Medley, A. L. Roquemore, D. K. Mansfield, R. V. Budny, M. P. Petrov, and R. E. Olson, Phys. Rev. Lett. **75**, 846 (1995).
[11] G. Manfredi and R. O. Dendy, Phys. Rev. Lett. **76**, 4360 (1996).
[12] R. Kleva and J. F. Drake, Phys. Fluids **27**, 1686 (1984).
[13] M. Pettini, A. Vulpiani, J. H. Misguich, M. De Leener, J. Orban, and R. Balescu, Phys. Rev. A **38**, 344 (1988).
[14] W. Horton, Plasma Phys. Controlled Fusion **27**, 937 (1985).
[15] W. Horton and D.-I. Choi, Plasma Phys. Controlled Fusion **29**, 901 (1987).
[16] M. Ottaviani, Europhys. Lett. **20**, 111 (1992).
[17] J. H. Misguich, R. Balescu, H. L. Pécseli, T. Mikkelsen, S. E. Larsen, and Q. Xiaoming, Plasma Phys. Controlled Fusion **29**, 825 (1987).
[18] M. B. Isichenko, Ya. L. Kalda, E. B. Tatarinova, O. V. Tel'kovskaya, and V. V. Yan'kov, Sov. Phys. JETP **69**, 517 (1989) [Zh. Eksp. Teor. Fiz. **96**, 913 (1989)].
[19] A. V. Gruznikov, M. B. Isichenko, and Ya. L. Kalda, Sov. Phys. JETP **70**, 263 (1990) [Zh. Eksp. Teor. Fiz. **97**, 476 (1990)].
[20] R. H. Kraichnan and D. Montgomery, Rep. Prog. Phys. **43**, 548 (1980).
[21] U. Frisch, *Turbulence* (Cambridge University Press, Cambridge, 1995), p. 240.
[22] A. Hasegawa, C. G. Maclennan, and Y. Kodama, Phys. Fluids **22**, 2122 (1979).
[23] W. W. Lee, J. Comput. Phys. **72**, 243 (1987).
[24] H. E. Mynick and J. A. Krommes, Phys. Rev. Lett. **43**, 1506 (1979).
[25] G. Knorr, F. R. Hansen, J. P. Lynov, H. L. Pécseli, and J. J. Rasmussen, Phys. Scr. **38**, 829 (1988).